



# Formation of Pt Skin Layer on Ordered and Disordered Pt-Co Alloys and Corrosion Resistance in Sulfuric Acid

Yu Sugawara<sup>1</sup> · Michiko Konno<sup>1,2</sup> · Izumi Muto<sup>1</sup> · Nobuyoshi Hara<sup>1</sup>

Published online: 18 December 2017

© The Author(s) 2017. This article is an open access publication

## Abstract

The formation of the Pt-enriched layer (Pt skin layer) formed at the surface of the ordered and disordered Pt-Co alloy specimens by a dealloying treatment and its corrosion resistance under potential cycling in sulfuric acid were examined to clarify the dissolution behavior of the Pt skin layer in polymer electrolyte fuel cell-operating conditions. The ordered and disordered Pt-Co specimens were obtained by heat treatment at 1073 and 1473 K, respectively. Co at the alloy surfaces dramatically dissolved in an early phase of the dealloying treatment in naturally aerated 0.5 M H<sub>2</sub>SO<sub>4</sub> at 298 K, and Pt skin layers were formed. Pt skin layers ca. 2 monolayer in thickness were formed on the Pt-Co alloy specimens by the dealloying treatment in 0.5 M H<sub>2</sub>SO<sub>4</sub>. The cyclic voltammetry measurements of the Pt-Co specimens showed the existence of Pt skin layers after the dealloying treatment and the inhibition of the Pt oxide formation on the Pt skin layers. The Pt oxide formation for ordered Pt-Co was more suppressed than that for the disordered Pt-Co. The Pt skin layers on the Pt-Co specimens exhibited a higher corrosion resistance than pure Pt, and the dissolution of the Pt skin layer for ordered Pt-Co was more inhibited than that for disordered Pt-Co under potential cycling in the potential range of 0.6–1.4 V in 0.5 M H<sub>2</sub>SO<sub>4</sub> (dissolution test). A thin, continuous Pt skin layer remained at the surface of the ordered Pt-Co specimen after the dissolution test. The formation of a uniform Pt skin layer seems to provide high oxidation resistance to the surface, leading to high corrosion resistance.

**Keywords** Pt-Co alloy · Pt skin layer · Order-disorder transition · Dissolution of Pt · Pt oxide formation

## Introduction

Polymer electrolyte fuel cells (PEFCs) have attracted attention as a power source of fuel cell vehicles (FCVs) and stationary power sources. Pt nanoparticles have been used as the cathode catalyst in PEFCs due to their high oxygen reduction reaction (ORR) activity and electrochemical stability over a wide potential range [1]. However, due to the cost and the limited supply of Pt, ORR activity has had to be enhanced to facilitate the widespread utilization of FCVs [1–3]. One of the solutions for the

improvement of ORR activity and the Pt utilization ratio is the use of Pt alloy catalysts. Many researchers have reported a higher ORR activity for binary and ternary alloys of Pt with 3d transition metals than for pure Pt [3–15]. Prior to the use of Pt alloy catalysts in PEFCs, because alloying elements dissolve from the catalyst and contaminate the proton exchange membrane [16], acid leaching treatment was commonplace [13, 17]. Acid leaching results in the formation of a Pt-enriched layer, referred to as a “Pt skin layer”, on the topmost surface of Pt alloy catalysts because of the instability of alloying elements. The enhancement of the ORR activity by alloying is attributed to the formation of the Pt skin layer; the change in the electronic structure of Pt atoms at the surface due to the existence of alloying elements in the sub-surface layer leads to a shift in the Pt *d*-band center, which affects the binding energy between adsorbed oxygenated species (OH, O) and the Pt surface [18–21]. The adsorption of oxygenated species which interfere with ORR on the Pt surface is thought to be suppressed at the Pt skin layer formed on Pt alloy catalysts in the potential region near the open-circuit voltage of PEFCs by the shift in the Pt *d*-band center [18, 22]. Among various Pt alloys, Pt-Co is a

✉ Yu Sugawara  
sugawaray@material.tohoku.ac.jp

<sup>1</sup> Department of Materials Science, Graduate School of Engineering, Tohoku University, 6-6-02, Aza-Aoba, Aramaki, Aoba-ku, Sendai 980-8579, Japan

<sup>2</sup> Present address: Steel Research Laboratories, Nippon Steel and Sumitomo Metal Corporation, 20-1, Shintomi, Futtsu, Chiba 293-8511, Japan

leading candidate for use as an alternative to Pt because it has the highest ORR activity; this is attributed to the appropriate arrangement of the Pt *d*-band center, as shown in experimental results and density function theory (DFT) simulations [23, 24]. In recent FCVs, Pt-Co nanoparticles were employed as the cathode catalyst [25, 26]. In recent years, researchers have focused on the optimization of the Pt-Co alloy catalyst with the aim of further enhancing the ORR activity, and the effectiveness of the ordered Pt-Co structure has been reported [27, 28].

With regard to the practical use of PEFCs, besides its ORR activity, the durability of the cathode catalysts is an important factor. Pt catalysts in the cathode are severely degraded under PEFC operation conditions; this is particularly true for potential cycling [29–32]. The dissolution of Pt occurs at the initial stage of the deterioration of Pt catalysts. Small Pt particles dissolve preferentially, and dissolved Pt ions are deposited on large Pt particles, which is referred to as “electrochemical Ostwald ripening” [33, 34]. This dissolution and redeposition processes result in the particle growth of Pt catalysts. The particle growth brings about the cell performance loss of PEFCs. In the case of Pt-Co alloy catalysts, the dissolution of Pt skin layers is important as it is with Pt catalysts. It has been reported that the dissolution of Pt skin layers and the redeposition of Pt ions cause the particle growth of Pt-Co catalysts and the thickening of Pt skin layers [35]. Because an increase in the thickness of Pt skin layer is known to weaken the benefit of Co addition to ORR activity, the dissolution of Pt skin layers is closely associated with the degradation of Pt-Co catalysts. The dissolution of alloying elements is an additional concern about Pt alloy catalysts [36, 37]. Some studies on the dissolution of alloying elements from Pt alloy electrodes have indicated that the dissolution of Pt skin layers triggers the dissolution of the alloying elements [38–40]; the corrosion resistance of the Pt skin layer formed on Pt-Co contributes enormously to the durability of Pt-Co alloy catalysts under the PEFC-operating condition. However, the dissolution behavior of the Pt skin layer in the simulated PEFC-operating conditions remains unclear because the corrosion resistance of the Pt skin layer cannot be evaluated by durability tests using Pt-Co nanoparticles. Therefore, a fundamental study using Pt-Co bulk electrodes regarding the corrosion resistance of the Pt skin layer is needed.

In this study, we conducted the dissolution tests of Pt-Co specimens under potential cycling in sulfuric acid. Prior to the dissolution tests, Pt skin layers were formed by simple immersion in sulfuric acid. In this process, the open-circuit potential of the specimens was monitored to examine the formation behavior of the Pt skin layers. We determined that the Pt skin layers were formed on the Pt-Co specimens and exhibited higher corrosion resistance than the pure Pt under potential cycling. In addition to this, because corrosion resistance is well-known to be sensitive to the microstructure of the specimen surface, we analyzed the effect of the order-disorder transition of the Pt-Co

alloy specimen on the dissolution of the Pt skin layers. Finally, the improvement mechanism of corrosion resistance for the Pt skin layers was discussed in terms of the morphology change of the Pt-Co specimen observed by scanning transmission electron microscope (STEM) and the Pt oxide formation behavior obtained by cyclic voltammetry (CV). To my knowledge, this study is the first challenge to measure the corrosion resistance of the Pt skin layer in the simulated PEFC-operating conditions. The results in this study will serve as a valuable contribution to the improvement of PEFC durability.

## Experimental

### Specimens and Electrolyte

Pt-Co alloy specimens were prepared from pure Pt (99.95 mass% purity) and pure Co (99.9 mass% purity) by ark melting under an Ar atmosphere. The molar ratio of Pt and Co in the specimens was 1:1. Pure Pt specimens were also employed for comparison. The specimens were cut into disks of 5 mm in thickness and 10 mm in diameter. The specimen surfaces were mechanically ground with 3000-grit SiC papers, without water, and then polished down to 0.25- $\mu\text{m}$  diamond paste. The specimens were ultrasonically cleaned with ethanol. After that, the specimens were heat-treated at 1073 or 1473 K for 43.2 ks under a vacuum-sealed condition in a silica glass tube to form the ordered or disordered structure of Pt-Co. In order to ensure the ordered structure, heat treatment was conducted at 1073 K, and the specimens were furnace-cooled. The specimens for the disordered structure were heat-treated at 1473 K, and the specimens were water-quenched. After heat treatment, the specimens were removed from the silica glass tube and electrochemical measurements were taken. An X-ray diffraction (XRD)  $\theta$ - $2\theta$  scan of the specimens was conducted to identify the ordered and disordered structures. A Bruker AXS D8 ADVANCE using Cu  $K\alpha$  radiation with a Ni filter was used for the XRD analysis.

The electrochemical measurements (dealloying treatment, CV, and dissolution test) were performed in 0.5 M  $\text{H}_2\text{SO}_4$  at 298 K. The electrolytes were made using ultra-pure deionized water (18.0  $\text{M}\Omega\text{ cm}$ ) and analytical-grade  $\text{H}_2\text{SO}_4$ .

### Dealloying Treatment

A simple immersion treatment for dealloying of the Pt-Co alloy specimens was conducted in naturally aerated 0.5 M  $\text{H}_2\text{SO}_4$  for 3.6 ks using a polychlorotrifluoroethylene (PCTFE) vessel to form the Pt skin layers on the specimen surfaces. In this treatment, the open-circuit potential of the specimen was measured. The reference electrode was a double junction Ag/AgCl (3.33 M KCl) with a saturated  $\text{K}_2\text{SO}_4$  salt bridge to prevent chloride contamination. In this paper, all potential values refer to the standard hydrogen electrode

(SHE). The electrolyte was sampled several times during the dealloying treatment to measure the amount of dissolved Pt and Co ions. Inductively coupled plasma-mass spectroscopy (ICP-MS) was used to measure the ion concentrations. An Agilent ICP-MS7500 was employed for the ICP-MS measurements. Tl and Ge elements were used as the internal standards for the quantitative determination of dissolved Pt and Co ions, respectively.

### Cyclic Voltammetry

CV measurements in the potential range of 0.05–1.4 V were performed in 0.5 M H<sub>2</sub>SO<sub>4</sub> deaerated by Ar in order to examine the electrochemical property of the dealloyed specimens. The specimen was sealed, with the exception of the working electrode surface, by a masking tape. The reference electrode was a Ag/AgCl (3.33 M KCl) with a saturated K<sub>2</sub>SO<sub>4</sub> salt bridge. A TOHO Technical Research PS-14 potentiostat and a Hokuto Denko HB-104 function generator were employed. Prior to the CV measurements, the specimen was polarized at 0.45 V for 60 s to remove an air-formed oxide, and the potential scan was started in the positive direction at 10 mV s<sup>-1</sup>.

### Dissolution Test by Potential Cycling

The dissolution tests were performed by the potential cycling in naturally aerated 0.5 M H<sub>2</sub>SO<sub>4</sub> using a three-electrode arrangement in a PCTFE vessel with 20-mL capacity. The number of cycling was 100 to investigate the initial stage of the degradation of Pt skin layers in the simulated PEFC conditions. The reference electrode was a Ag/AgCl (3.33 M KCl) with a saturated K<sub>2</sub>SO<sub>4</sub> salt bridge. A Au wire was used as the counterelectrode. The potential range of the CV was 0.6–1.4 V. An upper potential of 1.4 V was selected because cathode catalysts in PEFCs can be exposed to such high potentials by “reverse-current decay,” as was indicated by Reiser et al. [41]. In the dissolution test, the specimen was set to the PCTFE cell, and 18 mL of the electrolyte was introduced into the cell. The specimen was polarized at 0.6 V for 180 s to remove an air-formed oxide, and the dissolution test was started in the positive direction at 10 mV s<sup>-1</sup>. We confirmed that no dissolution of Pt occurred in the reduction process of the air-formed oxide [42]. After the dissolution test, the electrolyte was sampled to examine the amount of dissolved Pt and Co ions by ICP-MS. The sweep rate (10 mV s<sup>-1</sup>) was determined so that the amount of dissolved Pt could be fully detected by ICP-MS.

### Characterization of Pt Skin Layer at Pt-Co Specimen Surface

A JEOL JEM-ARM200F STEM system at an accelerating voltage of 200 kV was used to obtain the cross-sectional image of the specimen surface for the observation of the Pt skin

layers. The samples for STEM observation were prepared by focused ion beam (FIB) cross-sectioning. Prior to the FIB sample preparation for STEM, the crystal orientation of the specimens was determined by electron backscatter diffraction (EBSD), and the FIB micro-sampling was carried out at (111)-like grain. The EBSD analysis and the FIB sample preparation were performed by a JEOL JIB-4600F field emission-scanning electron microscope (FE-SEM) equipped with a dual-beam system.

The chemical shift of Pt by the formation of the Pt skin layer was investigated by angular-resolved X-ray photoelectron spectroscopy (XPS). A Thermo Fisher Scientific theta probe using a monochromated Al K $\alpha$  radiation at an accelerating voltage of 15 kV and an anode current of 30 mA was employed for the XPS measurements. The X-ray spot size was ca. 200  $\mu$ m, and the XPS measurements were carried out inside the single grain. The XPS spectra were calculated by integration of the spectra obtained in the XPS measurements at a detection angle of the photoelectrons of 21.875–78.125°. The binding energy of the XPS spectra was calibrated based on the peak position of the C–H bond in the C 1s level (285.00 eV), and the spectra was exhibited after the background spectra was subtracted from the original spectra by the nonlinear background subtraction method [43].

## Results and Discussion

### Ordered/Disordered Identification

To confirm the formation of ordered and disordered Pt-Co as a result of heat treatment, the Pt-Co specimens were subjected to an XRD analysis. The X-ray diffraction patterns of the specimens heat-treated at 1073 or 1473 K are shown in Fig. 1. All the peaks of the specimen heat-treated at 1073 K were assigned to the ordered PtCo phase (face-centered tetragonal (fct)  $a = 2.682$  Å,  $c = 3.675$  Å) [44], and no peaks of Pt, Co, and Pt<sub>3</sub>Co were observed. Also, all the peaks of the specimen heat-treated at 1473 K were assigned to the disordered PtCo phase (face-centered cubic (fcc)  $a = 3.835$  Å) [44]. These results indicate that the ordered fct and disordered fcc structures were successfully obtained by heat treatment. From the comparison between the fct and fcc structures of Pt-Co alloy, the positions of Pt and Co atoms differ depending on the crystal structure, suggesting the formation behavior of Pt skin layers on the ordered Pt-Co differs from that of disordered Pt-Co.

### Pt Skin Layer Formation by the Dealloying Treatment

Pt skin layers were formed by simple immersion in 0.5 M H<sub>2</sub>SO<sub>4</sub>. The open-circuit potential of the ordered Pt-Co specimen during the dealloying treatment is indicated in Fig. 2a.

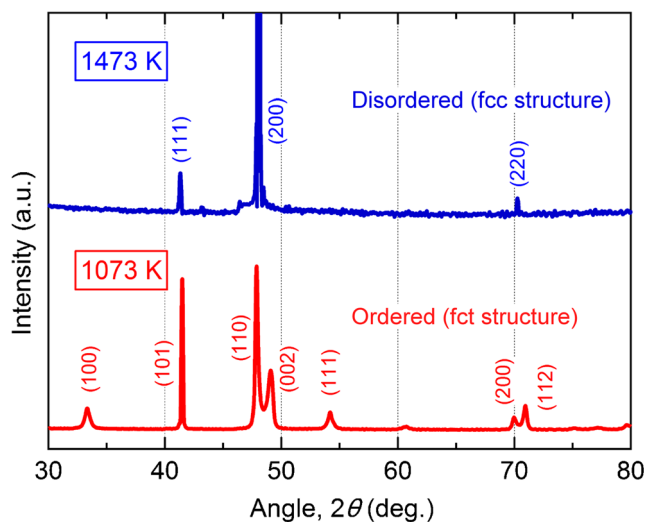


**Fig. 1** X-ray diffraction patterns of Pt-Co specimens heat-treated at 1073 or 1473 K for 43.2 ks. The ordered phase with fct structure and the disordered one with fcc structure were obtained by heat treatment at 1073 and 1473 K, respectively

The open circuit potential of the pure Pt specimen is also exhibited in Fig. 2a for comparison. The inset in Fig. 2a is an enlarged view of the initial stage. At the beginning of the dealloying treatment, the open-circuit potential of the ordered Pt-Co specimen was ca. 0.0 V, and it increased rapidly to ca.

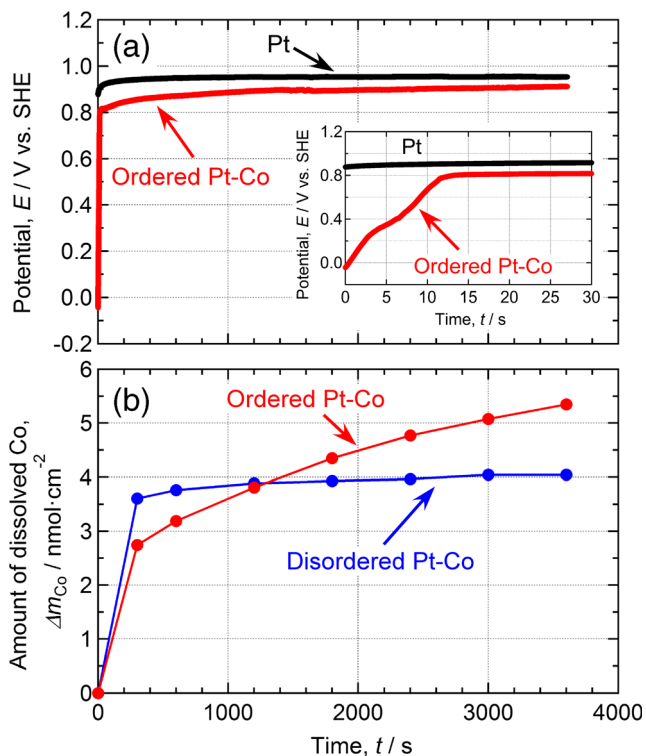


**Fig. 2** **a** Open-circuit potentials of the pure Pt and ordered Pt-Co specimens as a function of immersion time in naturally aerated 0.5 M H<sub>2</sub>SO<sub>4</sub> at 298 K. Inset: the enlarged view in the initial stage. **b** Changes in the amount of dissolved Co for the ordered and disordered Pt-Co specimens during dealloying treatment in naturally aerated 0.5 M H<sub>2</sub>SO<sub>4</sub> at 298 K

0.8 V for 12 s. After 12 s, a slowdown was noted in the increase rate of the potential, and a steady-state value was achieved. The increase in the open-circuit potential was likely due to the selective dissolution of Co from the surface of the Pt-Co specimen. From the thermodynamic data, the equilibrium potential of the Pt dissolution (Eq. 1) is 1.188 V, and that of the Co dissolution (Eq. 2) is −0.277 V [45].



This indicates that Co dissolves above ca. −0.28 V. On the other hand, little dissolution of Pt occurs below ca. 1.2 V. The selective dissolution of Co from the Pt-Co specimen tends to occur in the potential range of −0.28–1.2 V. Moreover, when Co dissolves selectively and a Pt skin layer is generated on the specimen surface, the open-circuit potential of Pt-Co approaches the equilibrium potential of Pt dissolution presented in Eq. 1. Because the open-circuit potential of the ordered Pt-Co specimen shifted positively at the beginning of the dealloying treatment, as shown in Fig. 2a, and the steady-state value was close to the equilibrium potential of Pt dissolution, it was suggested that the Co dissolved selectively and the Pt skin layer subsequently formed.

In order to confirm the selective dissolution of Co, the amount of dissolved Co was measured. Figure 2b represents the changes in the amount of dissolved Co for the ordered and disordered Pt-Co specimens during the dealloying treatment. As shown in Fig. 2b, the concentrations of Co ions for the ordered and disordered Pt-Co specimens rapidly increased during the initial stage of the immersion (0–300 s). It was expected that Co at the alloy surfaces would drastically dissolve in the early phase of the dealloying treatment. After 300 s, the dissolution rate of Co in the ordered specimen was higher than that in the disordered one. Consequently, the total amount of the dissolved Co from the ordered Pt-Co specimen in the dealloying treatment was higher than that from the disordered Pt-Co specimen. This affected the surface roughness of the specimens. However, as described later, no surface roughness was thought to influence the corrosion resistance of the Pt skin layers.

The dissolution amounts of Pt and Co for the ordered and disordered Pt-Co in the dealloying treatment (after 3.6 ks) are listed in Table 1. For the ordered Pt-Co specimen, the molar amounts of the dissolved Pt and Co were 0.36 and 5.4 nmol cm<sup>−2</sup>, and those for the disordered one were 0.015 and 4.1 nmol cm<sup>−2</sup>, respectively. For both specimens, the total amounts of the dissolved Pt were one or two orders of magnitude smaller than those of Co. These results suggest that the selective dissolution of Co occurred during the dealloying treatment in 0.5 M H<sub>2</sub>SO<sub>4</sub>.

On the basis of the data shown in Table 1, the thickness of the Pt skin layers for the Pt-Co specimens was estimated to be

**Table 1** Molar amounts of dissolved Pt and Co for the ordered Pt and disordered Pt-Co specimens during the dealloying treatment in naturally aerated 0.5 M H<sub>2</sub>SO<sub>4</sub> at 298 K

	Amount of dissolved Pt, $\Delta m_{\text{Pt}}$ (nmol cm <sup>-2</sup> )	Amount of dissolved Co	
		$\Delta m_{\text{Co}}$ (nmol cm <sup>-2</sup> )	$\Delta m_{\text{Co}}$ (monolayer)
Ordered Pt-Co	0.36 (SD = 0.16)	5.4 (SD = 0.43)	3.7
Disordered Pt-Co	0.015 (SD = 0.003)	4.1 (SD = 0.84)	3.2

SD standard deviation

ca. 2 monolayer (ML). If a single ML of ordered Pt-Co(111) phase dissolves, the amount of the dissolved Co is equivalent to ca. 86 ng cm<sup>-2</sup>. The actual amount of the dissolved Co was 316 ng cm<sup>-2</sup>; hence, ca. 3.7 ML of the Pt-Co alloy dissolved during the dealloying treatment. For the disordered Pt-Co alloy, the Co dissolution of a single ML of Pt-Co(111) phase corresponds to ca. 75 ng cm<sup>-2</sup>. The actual amount of the dissolved Co was 239 ng cm<sup>-2</sup>; thus, ca. 3.2 ML of Pt-Co alloy dissolved. In the calculation of the thickness of Pt skin layers, it was assumed that all the Pt atoms remained on the surface because the trace amounts of the Pt dissolution were observed on both specimens. From this prediction, the thickness of the Pt skin layers formed on both alloys was ca. 2 ML. A Pt skin layer of 2 ML in thickness is equivalent to that formed on Pt-Co nanoparticles used as catalysts in PEFCs [35].

### XPS Investigation of the Formation of Pt Skin Layer

Directly observing whether Pt skin layers formed on the bulk Pt-Co alloy was difficult because the layers were expected to be extremely thin. In order to confirm the existence of the Pt skin layers on the ordered and disordered Pt-Co specimens, a XPS analysis was conducted. Figure 3 shows the Pt 4f XPS spectra of the as-polished pure Pt and the ordered and disordered Pt-Co specimens that were treated with dealloying treatment. The Pt 4f<sub>7/2</sub> and Pt 4f<sub>5/2</sub> peaks were observed around 72 and 75 eV, respectively. A slight shift in the Pt 4f<sub>7/2</sub> and Pt 4f<sub>5/2</sub> peaks for the ordered and disordered Pt-Co specimens to higher binding energies was noted than those of the pure Pt specimen. The chemical shift of the Pt 4f XPS spectra for the Pt-Co alloys shown in Fig. 3 agrees with the literature [46, 47]. This was attributed to the electron transfer from Co to Pt at the surfaces induced by the formation of the Pt skin layer. The increase in the electron energy of the d-band of Pt leads to an increase in the Fermi level ( $E_F$ ). As a result, a positive shift in the Pt 4f binding energy referenced to  $E_F$  was detected in the XPS spectra [48]. The Pt 4f core level shift cannot be observed when a thick Pt skin layer is formed [18]. Hence, it was concluded that the dealloying treatment in this study produced a

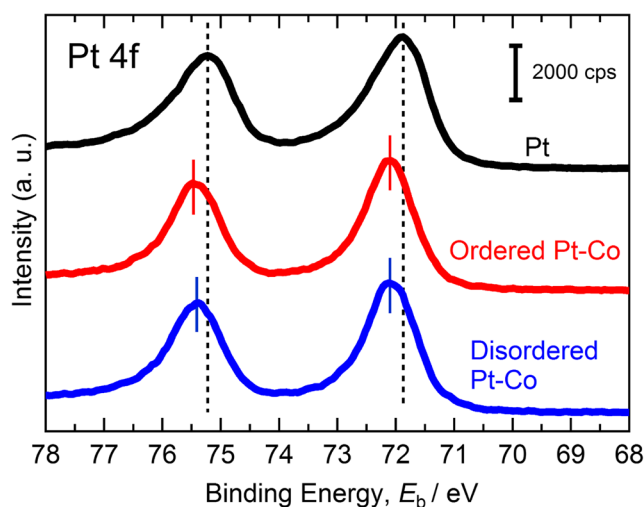


**Fig. 3** Pt 4f XPS spectra of the pure Pt, ordered Pt-Co, and disordered Pt-Co specimens. The XPS measurements of the ordered Pt-Co and disordered Pt-Co specimens were carried out after the dealloying treatment

few megalangmuir of the Pt at the surface of the Pt-Co specimens.

### Electrochemical Property of Pt Skin Layer Formed at the Pt-Co Surface

CV measurements in deaerated 0.5 M H<sub>2</sub>SO<sub>4</sub> were performed to investigate the electrochemical properties of the Pt skin layers formed by dealloying treatment. Figure 4 shows the CVs of the ordered and disordered Pt-Co specimens after dealloying treatment. As a reference, the CV of the as-polished Pt is presented. Pt skin layers on Pt-Co alloys have the different hydrogen adsorption properties of pure Pt [49, 50]; thus, the geometric surface area was regarded as the electrode surface area for the disordered Pt-Co and pure Pt

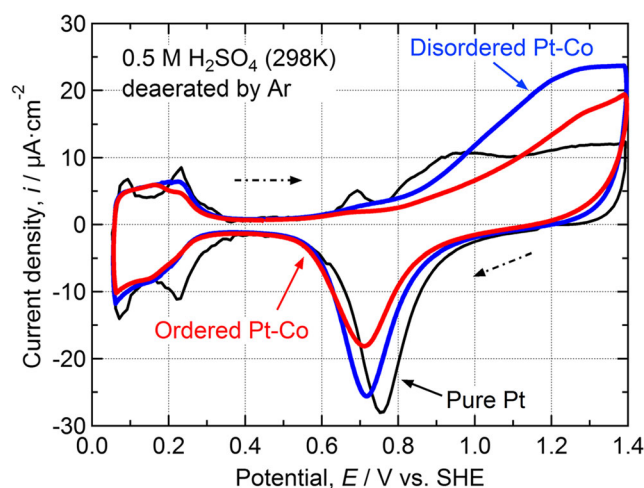
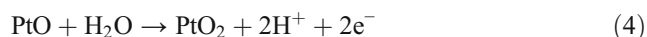
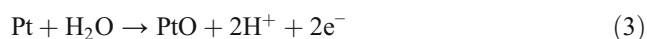


**Fig. 4** Cyclic voltammograms (CVs) of the ordered Pt-Co, disordered Pt-Co, and pure Pt specimens measured at a scan rate of 10 mV s<sup>-1</sup> in deaerated 0.5 M H<sub>2</sub>SO<sub>4</sub> at 298 K. The CVs of the ordered Pt-Co and disordered Pt-Co specimens were obtained after the dealloying treatment

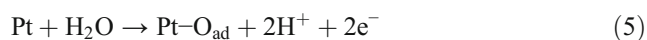
specimens. The ordered Pt-Co specimens had relatively rough surfaces compared with the disordered ones because the amount of dissolved Co from the ordered Pt-Co during the dealloying treatment was larger than that for the disordered one. Therefore, the electrode surface area for the ordered Pt-Co specimens was determined by multiplying the geometric surface area by the charge ratio for the hydrogen adsorption derived from the CVs of the ordered and disordered Pt-Co. As shown in Fig. 4, the CV of the ordered Pt-Co specimen was similar to that of the disordered Pt-Co specimen. In addition to this, the voltammogram of the ordered and disordered Pt-Co specimens were similar to that for the pure Pt specimen. It can be therefore assumed that the CV measurements indicated that the electrochemical behavior of the ordered and disordered Pt-Co specimens after dealloying treatment was analogous to that of the pure Pt specimen. These results are evidence that Pt skin layers were formed at the ordered and disordered Pt-Co surfaces due to dealloying treatment.

The typical CV of Pt electrodes is characterized by a region for hydrogen adsorption and desorption below 0.4 V, and Pt oxide formation and its reduction appear in the potential range of 0.4–1.4 V [51]. As shown in Fig. 4, the peaks for hydrogen adsorption and desorption were clearly observed on the pure Pt electrode. On the other hand, the absence of obvious peaks on the Pt-Co electrodes suggests that the hydrogen adsorption property was altered by the formation of the Pt skin layers [49, 50].

In general, PtO and PtO<sub>2</sub> are formed by the oxidation of Pt [52, 53]:



Besides Pt oxide formation and its reduction, the adsorption of the oxygen species at the surface (Pt-OH<sub>ad</sub> and Pt-O<sub>ad</sub>) [54, 55] occurs simultaneously. Adsorbed oxygen species such as Pt-O<sub>ad</sub> are produced by the oxidation of H<sub>2</sub>O:



We described the Pt oxides and the adsorbed oxygen species as “Pt-O” collectively in this paper. In addition, the oxidation peak around 0.7 V for the pure Pt specimen was unusual. We think that the oxidation peak might be a kind of the Pt-O formation. Figure 4 shows that the start of the Pt-O formation shifted to the anodic direction in the order of the pure Pt, disordered Pt-Co, and ordered Pt-Co. In addition, the peak of the Pt-O reduction in the negative scan of 1.2 → 0.4 V became smaller in the same order.

The start of Pt-O formation is evaluated using the parameter  $E_{10 \mu\text{A cm}^{-2}}$ , which is the potential where the current density reached 10  $\mu\text{A cm}^{-2}$  in the potential scan of 0.5 → 1.4 V.  $E_{10 \mu\text{A cm}^{-2}}$  and the amount of the reduction charge of Pt-O ( $Q_{\text{Red}}$ ) are listed in Table 2.  $Q_{\text{Red}}$  was calculated in the

**Table 2** Potential at 10  $\mu\text{A cm}^{-2}$  in the Pt-O formation region ( $E_{10 \mu\text{A cm}^{-2}}$ ) and the amount of reduction charge of Pt-O ( $Q_{\text{Red}}$ ) obtained from the CVs in Fig. 4. The potential at 10  $\mu\text{A cm}^{-2}$  was evaluated from the anodic current in the positive scan in the potential range of 0.6–1.4 V. The reduction charge was calculated in the negative scan in the potential range of 1.2–0.4 V

	Potential at 10 $\mu\text{A cm}^{-2}$ , $E_{10 \mu\text{A cm}^{-2}}$ (V vs. SHE)	Reduction charge of Pt-O, $Q_{\text{Red}}$ ( $\mu\text{C cm}^{-2}$ )
Ordered Pt-Co	1.11	323
Disordered Pt-Co	0.97	432
Pure Pt	0.91	451

potential scan of 1.2 → 0.4 V. Table 2 indicates that the start of the Pt-O formation for the ordered Pt-Co was effectively delayed, beginning 0.2 V later than in the case of the pure Pt specimen. Moreover, the amount of the Pt-O formation on the ordered Pt-Co was 70–75% less than that on the pure Pt and disordered Pt-Co. This implies that the Pt skin layers formed on the ordered Pt-Co exhibited a higher resistance to Pt-O formation than the pure Pt and disordered Pt-Co.

In Fig. 2 and Table 1, the amounts of Pt and Co dissolutions for the ordered Pt-Co were larger than those for the disordered Pt-Co in the dealloying treatment. However, it was found that the Pt skin layer formed on the ordered Pt-Co alloy had a higher resistance to surface oxidation than that on the disordered Pt-Co alloy.

### Corrosion Resistance of Pt Skin Layer Under the Potential Cycling

In order to examine the corrosion resistance of the Pt skin layers on the Pt-Co specimens in the simulated PEFC conditions, a dissolution test was conducted after the formation of the Pt skin layers. The molar amount of the dissolved Pt from the ordered and disordered Pt-Co specimens is shown in Fig. 5 with the result for the pure Pt specimen. The results clearly reveal that the inhibition of the dissolution of the Pt skin layer was higher than that of the pure Pt. Moreover, the amount of dissolved Pt for the ordered Pt-Co was smaller than for the disordered one. This leads us to conclude that the enhancement of the corrosion resistance by the formation of the Pt skin layer provides Pt-Co alloy catalysts with high durability. These results indicate that Pt alloy catalysts, such as Pt-Co and Pt-Cu, are more durable than commercial Pt catalysts in the PEFC cathode conditions [56–58].

The amounts of the dissolved Pt and Co during the dissolution test are summarized in Table 3. If a single ML of Pt(111) phase dissolves, the amount of the dissolved Pt is 483  $\text{ng cm}^{-2}$ . In addition, if a single ML of Pt skin layers on ordered and disordered Pt-Co(111) phases dissolves, the amount of the dissolved Pt is equivalent to ca. 580 and 505  $\text{ng cm}^{-2}$ , respectively.

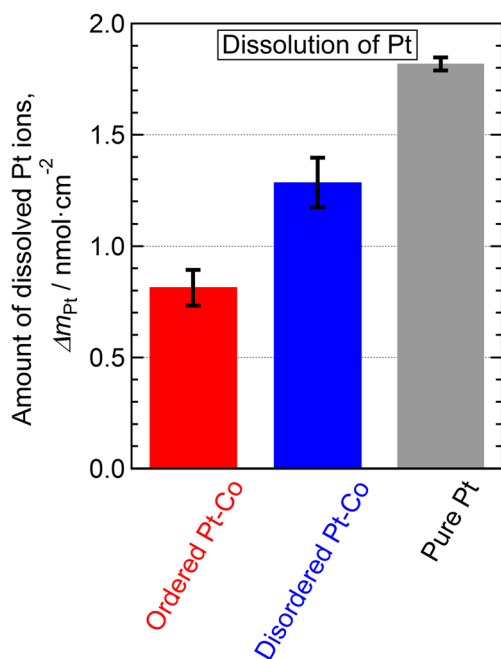


**Fig. 5** Amount of dissolved Pt for the ordered Pt-Co, disordered Pt-Co, and pure Pt specimens during the dissolution test in naturally aerated 0.5 M H<sub>2</sub>SO<sub>4</sub> at 298 K. The dissolution test: 100 cycles of the potential cycling in the potential range of 0.6–1.4 V at 10 mV s<sup>-1</sup>. The dissolution tests with the ordered and disordered Pt-Co specimens were carried out after the dealloying treatment

Hence, the amounts of dissolved Pt from the ordered Pt-Co, disordered Pt-Co, and pure Pt specimens during the dissolution test correspond to ca. 0.27, 0.50, and 0.73 ML, respectively. Because nanoparticle catalysts deteriorate in the PEFCs due to the atomic-scale dissolution of Pt, the formation of the Pt skin layers is expected to contribute to the improvement of the cell performance of PEFCs.

As shown in Table 3, there was no significant difference in the amount of the dissolved Co between the ordered and disordered Pt-Co specimens. For the ordered Pt-Co specimen, the molar amounts of the dissolved Pt and Co were 0.81 and 3.4 nmol cm<sup>-2</sup>, respectively. For the disordered Pt-Co specimen, the molar amounts of the dissolved Pt and Co were 1.3 and 3.9 nmol cm<sup>-2</sup>, respectively. It was indicated that the dissolution of a single Pt atom from the ordered and disordered Pt-Co brought about ca. four and three atoms of Co dissolution. A Pt skin layer ca. 2 ML in thickness was

expected to be formed on the Pt-Co specimen by dealloying. The dissolution of Co during the dissolution test means that the Pt skin layer was thickened and repaired during the dissolution test.

After the dissolution test, CV measurements in deaerated 0.5 M H<sub>2</sub>SO<sub>4</sub> were performed to examine the change in the electrochemical properties due to the dissolution test. Figure 6 shows the CVs of the ordered and disordered Pt-Co specimens before and after the dissolution test. The enlarged current densities can be seen due to the dissolution test; this implies that potential cycling thickened the Pt skin layer and the electrochemical properties of the Pt-Co specimens approached that of the pure Pt specimen.

In order to evaluate the change of the Pt-O formation behavior by the dissolution test, the potential at 10 μA cm<sup>-2</sup> in the Pt-O formation region ( $E_{10 \mu\text{A cm}^{-2}}$ ) and the amount of the reduction charge of Pt-O ( $Q_{\text{Red}}$ ) after the dissolution test calculated from the CVs in Fig. 6 are listed in Table 4. A comparison of Tables 2 and 4 indicates a slight shift in  $E_{10 \mu\text{A cm}^{-2}}$  to negative values (1.11 → 1.05 V for the ordered, 0.97 → 0.95 V for the disordered Pt-Co) and a clear increase in  $Q_{\text{Red}}$  (323 → 390 μA cm<sup>-2</sup> for the ordered, 432 → 456 μA cm<sup>-2</sup> for the disordered Pt-Co) due to the dissolution test. The values of  $Q_{\text{Red}}$  for the disordered Pt-Co specimen after the dissolution test and the pure Pt specimen were similar, suggesting that a positive effect of Co addition on the catalytic activity for the disordered Pt-Co disappeared. The CV of the disordered Pt-Co specimen after the dissolution test indicated the relatively sharp peaks in the hydrogen adsorption and desorption regions, which also suggests that the electrochemical properties approached that of the pure Pt [49]. Hence, it can be concluded that the corrosion resistance and the durability of the cathode catalyst in PEFCs for the ordered Pt-Co alloy are higher than those for the disordered Pt-Co alloy. The reason for the advantage of the ordered Pt-Co in terms of durability seemed to be attributed to the difference in the morphology and structure of the Pt skin layers.

The cross sections of the Pt-Co specimen surfaces were observed by STEM to gain morphological information of the Pt skin layers after the dissolution test. The cross-sectional STEM-HAADF (high-angle annular dark field) images of the ordered and disordered Pt-Co specimen surfaces after the dissolution test are shown in Fig. 7. A carbon coating

**Table 3** Molar amounts of dissolved Pt and Co for the ordered Pt-Co, disordered Pt-Co, and pure Pt specimens during the dissolution test in naturally aerated 0.5 M H<sub>2</sub>SO<sub>4</sub> at 298 K

	Amount of dissolved Pt		Amount of dissolved Co, $\Delta m_{\text{Co}}$ (nmol cm <sup>-2</sup> )
	$\Delta m_{\text{Pt}}$ (nmol cm <sup>-2</sup> )	$\Delta m_{\text{Pt}}$ (monolayer)	
Ordered Pt-Co	0.81 (SD = 0.08)	0.27	3.4 (SD = 0.55)
Disordered Pt-Co	1.3 (SD = 0.11)	0.50	3.9 (SD = 0.25)
Pure Pt	1.8 (SD = 0.03)	0.73	–

SD standard deviation

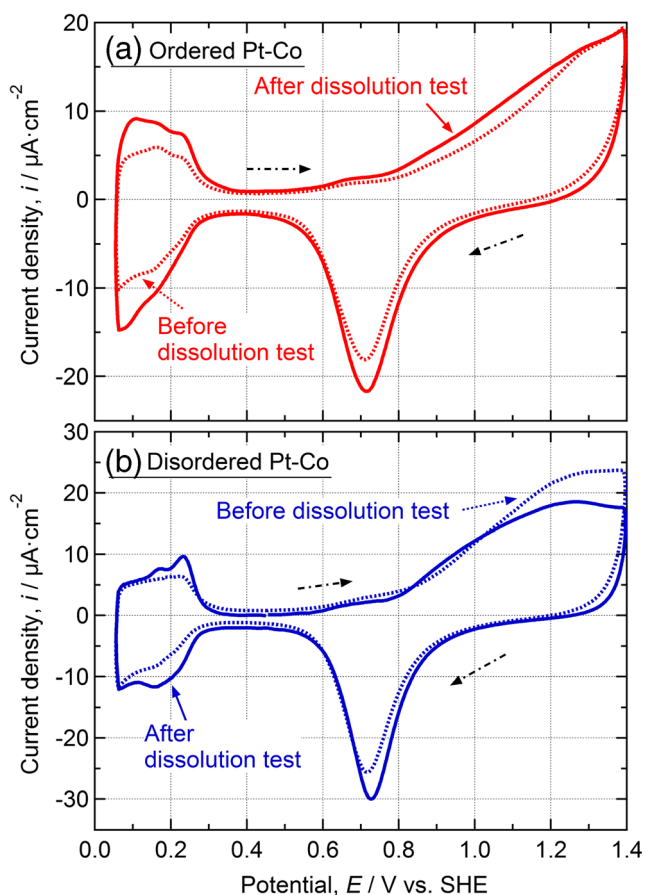


**Fig. 6** Cyclic voltammograms (CVs) of the ordered and disordered Pt-Co specimens obtained before and after the dissolution test. The CVs were measured at a scan rate of  $10 \text{ mV s}^{-1}$  in deaerated  $0.5 \text{ M H}_2\text{SO}_4$  at  $298 \text{ K}$

was performed on the surface of the specimens. The black parts in the upper sides of Fig. 7 correspond to the carbon layers. The Pt-enriched zone appears as a white region because the contrast in the HAADF images is reflected by the difference in the average atomic weights of Pt and Pt-Co. As shown in Fig. 7b, a discontinuous white layer of ca. 1–1.5 nm in thickness could be observed at the surface of the disordered Pt-Co specimen. This white layer must be the Pt skin layer; it was found that a discontinuous Pt skin layer was distributed at the disordered Pt-Co surface after the dissolution test. On the other hand, no obvious contrast was observed at the surface of the ordered Pt-Co shown in Fig. 7a, suggesting that the

**Table 4** Potential at  $10 \mu\text{A cm}^{-2}$  in the Pt-O formation region ( $E_{10 \mu\text{A cm}^{-2}}$ ) and amount of reduction charge of Pt-O ( $Q_{\text{Red}}$ ) after the dissolution test obtained from the CVs in Fig. 6

	Potential at $10 \mu\text{A cm}^{-2}$ , $E_{10 \mu\text{A cm}^{-2}}$ (V vs. SHE)	Reduction charge of Pt-O, $Q_{\text{Red}}$ ( $\mu\text{C cm}^{-2}$ )
Ordered Pt-Co	1.05	390
Disordered Pt-Co	0.95	456

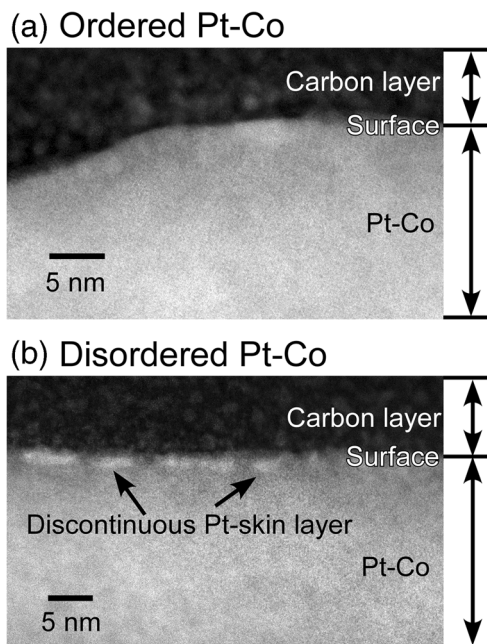


**Fig. 7** Cross-sectional STEM-HAADF images of **a** the ordered and **b** disordered Pt-Co specimen surfaces after the dissolution test

specimen maintained a very thin Pt skin layer during the dissolution test. The difference in the morphology of the Pt skin layer between the ordered and disordered Pt-Co specimens shown in the HAADF observations were consistent with those expected from the results in Fig. 6. As shown in Fig. 6b, the CV of the disordered Pt-Co after the dissolution test denoted asymmetric current behavior in the hydrogen adsorption and desorption regions, which suggests discontinuity in the Pt skin layer over the surface [46, 59]. It has been reported that the formation of continuous Pt skin layers at the surface of Pt alloy nanoparticles by the heat treatments provided the inhibition of the Pt-O formation and the enhancement of the ORR activity [60–62]. This implies that a thin and continuous Pt skin layer was formed on the ordered Pt-Co surface. The formation of a uniform Pt skin layer is a key point in the corrosion resistance of Pt-Co specimens.

### Improvement Mechanism of Corrosion Resistance of Pt Skin Layer

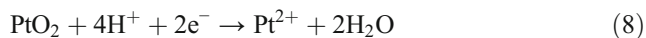
As mentioned in an earlier section, the Pt skin layers formed at the Pt-Co alloy surfaces were found to provide better corrosion resistance than the pure Pt. It was also found that corrosion resistance of the Pt skin layer formed at the ordered Pt-Co surface was higher than that at the disordered Pt-Co surface. In addition, a thin and continuous Pt skin layer was formed on the ordered Pt-Co surface, and the barrier effect of the Pt skin layer on the Pt-O formation was maintained after the dissolution test. These results suggest that the high corrosion resistance of the Pt skin layer is closely related to the suppression of Pt-O formation.



In previous study and in some papers on the dissolution of Pt in acid solutions, the protective and detrimental effects of the Pt oxides on the dissolution of polycrystalline Pt were reported. Because the chemical dissolution rate of the Pt oxides is extremely low, the Pt oxides behave as the passive film under potentiostatic conditions [42, 63–65]. On the other hand, an increase in the amount of Pt dissolution was observed with increased coverage of the Pt oxides under potentiodynamic conditions, such as during potential cycling [42, 66–77]. During the anodic potential scan, the Pt-O coverage increases as the potential increases, and a repulsive interaction between adsorbed O atoms at Pt surfaces is generated. Energetically unstable O atoms at the surface enter the sub-surface site of Pt, which is energetically favorable. This is a so-called place exchange [52, 78–80]. The place exchange between Pt and O atoms was confirmed by an X-ray absorption fine structure (XAFS) spectroscopy measurement [54] and a scanning tunneling microscopy (STM) observation [81]. It seems that the Pt–Pt bond is weakened by the place exchange and the following anodic dissolution reactions of Pt occur:



Some researchers pointed out that the place exchange triggers the anodic dissolution of Pt [42, 68, 71, 76]. In addition, PtO<sub>2</sub> is formed when the anodic potential limit of potential cycling is more than 1.2 V, and Pt reductively dissolves during the cathodic potential scan [42, 72, 76, 82–84]:



In the case of the potential range of 0.6–1.4 V in this study, both anodic and cathodic dissolutions were possible. PtO<sub>2</sub> is an oxide with a 3-D structure [85, 86] and is produced via place exchange. Therefore, place exchange is the key factor in the dissolution of Pt. Because place exchange accelerated as the coverage of Pt-O increased, the inhibition of the Pt-O formation effectively suppressed the dissolution of Pt.

As shown in Fig. 4, the Pt skin layer was more resistant to Pt-O formation than the pure Pt. Particularly, the durability of the thin and continuous Pt skin layer formed on the ordered Pt-Co was especially high with regard to surface oxidation. By taking the mechanism of the Pt dissolution via the Pt oxide formation into account, the high resistance to the Pt-O formation can be considered to be the main reason for the superior corrosion resistance of the Pt skin layer.

Figure 8 shows the effect of the thickness of Pt-O on the dissolution of Pt during the dissolution test. The thickness of the Pt-O was obtained from the average values of the reduction charges of the Pt-O before and after the dissolution test shown in Tables 2 and 4. As denoted in Fig. 8, the amount of the dissolved Pt was suppressed as the thickness of the Pt-O

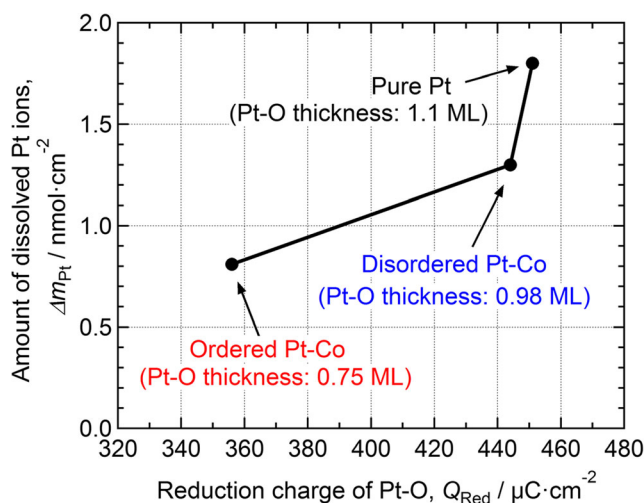


**Fig. 8** Effect of the reduction charge of Pt-O on the amount of the dissolution of Pt during the dissolution test

decreased. This indicates that the improvement in the corrosion resistance of the Pt skin layers is caused by the inhibition of the Pt-O formation. In addition, Fig. 8 suggests that the dissolution of Pt is likely to be accelerated by the formation of more than a single ML of the Pt-O. The increase in the thickness of the Pt-O promotes place exchange and subsequent PtO<sub>2</sub> formation, which accelerates the dissolution of Pt. The Pt-O formation on the ordered and disordered Pt-Co specimens did not reach 1 ML; thus, the place exchange and the PtO<sub>2</sub> formation were thought to be inhibited. Imai et al. and Gu et al. reported that Pt-Co nanoparticles suppress the place exchange and the formation of the Pt oxide with a 3-D structure, such as PtO<sub>2</sub>, by XAFS analysis [87] and DFT calculations [88]. An EQCM study using Pt-Cu electrocatalysts by Mathew et al. also supported the barrier effect of the Pt skin layer on Pt surface oxidation [89].

In this study, we demonstrated the high corrosion resistance of the Pt skin layer formed on the ordered Pt-Co specimen under the potential cycling condition simulating the operation of PEFCs. This is due to the high surface oxidation resistance of the Pt skin layer by the *d*-band shift. Pt-Co catalysts are expected to provide a positive effect not only on the ORR activity but also on the durability of PEFCs by the formation of Pt skin layers.

## Conclusions

The formation of the Pt skin layers formed at the surface of the ordered and disordered Pt-Co alloy specimens by the dealloying treatment and its corrosion resistance under the potential cycling were examined to elucidate the dissolution behavior of the Pt skin layer in the PEFC-operating conditions. The following conclusions were derived.

The ordered and disordered Pt-Co specimens were successfully obtained by heat treatment at 1073 and 1473 K,

respectively. Co at the alloy surfaces dramatically dissolved in an early stage during the dealloying treatment in naturally aerated 0.5 M H<sub>2</sub>SO<sub>4</sub> at 298 K, and the Pt skin layers were formed. The thickness of the Pt skin layers formed at the Pt-Co surfaces were estimated at ca. 2 monolayer. The CV measurements after the dealloying treatment indicated that the Pt skin layers suppressed the Pt-O formation in the PEFC cathode condition. The resistance of the ordered Pt-Co to Pt-O formation was higher than that of the disordered Pt-Co. The dissolution amount of the Pt skin layer was less than that of the pure Pt during the dissolution test. The suppression of the Pt-O formation can be considered the main reason for the high corrosion resistance of Pt skin layers. In the case of ordered Pt-Co, the dissolution of the Pt skin layer was highly suppressed compared with the disordered Pt-Co. The ordered Pt-Co specimen maintained the thin and continuous Pt skin layer after the dissolution test. The formation of the uniform Pt skin layer is an important factor in preventing the dissolution of Pt.

**Acknowledgments** Y. S. would like to acknowledge Prof. T. Wadayama and Prof. N. Todoroki for the fruitful discussion.

**Funding Information** This work was supported by JSPS KAKENHI Grant Numbers JP23760685 and JP15H05550.

**Open Access** This article is distributed under the terms of the Creative Commons Attribution 4.0 International License (<http://creativecommons.org/licenses/by/4.0/>), which permits unrestricted use, distribution, and reproduction in any medium, provided you give appropriate credit to the original author(s) and the source, provide a link to the Creative Commons license, and indicate if changes were made.

## References

- M.K. Debe, *Nature* **486**, 43 (2012)
- C. Jaffray, in *Handbook of fuel cells fundamentals, technology and applications*, ed. by W. Vielstich, A. Lamm, H. A. Gasteiger. (John Wiley & Sons, Chichester, 2003), p. 509
- H.A. Gasteiger, N.M. Marković, *Science* **324**, 48 (2009)
- H. Liu, D. Xia, J. Zhang, in *PEM fuel cell electrocatalysts and catalyst layers*, ed. by J. Zhang. (Springer-Verlag, London, 2008), p. 631
- L. Gan, P. Strasser, in *Electrocatalysis in fuel cells*, ed. by M. Shao. (Springer-Verlag, London, 2013), p. 536
- T.R. Ralph, M.P. Hogarth, *Platin. Met. Rev.* **46**, 3 (2002)
- T. Toda, H. Igarashi, H. Uchida, M. Watanabe, *J. Electrochem. Soc.* **146**, 3750 (1999)
- M. Watanabe, D.A. Tryk, M. Wakisaka, H. Yano, H. Uchida, *Electrochim. Acta* **84**, 187 (2012)
- S. Mukerjee, S. Srinivasan, M.P. Sorinaga, *J. Phys. Chem.* **99**, 4577 (1995)
- S. Mukerjee, S. Srinivasan, M.P. Sorinaga, *J. Electrochem. Soc.* **142**, 1409 (1995)
- N.M. Marković, T.J. Schmidt, V. Stamenković, P.N. Ross, *Fuel Cells* **1**, 105 (2001)
- U.A. Paulus, A. Wokaun, G.G. Scherer, T.J. Schmidt, V. Stamenković, N.M. Marković, P.N. Ross, *Electrochim. Acta* **47**, 3787 (2002)
- H.A. Gasteiger, S.S. Kocha, B. Sompalli, F.T. Wagner, *Appl. Catal. B. Environ.* **56**, 9 (2005)
- S. Koh, N. Hahn, C. Yu, P. Strasser, *J. Electrochem. Soc.* **155**, B1281 (2008)
- T. Wadayama, H. Yoshida, K. Ogawa, N. Todoroki, Y. Yamada, K. Miyamoto, Y. Iijima, T. Sugawara, K. Arihara, S. Sugawara, K. Shinohara, *J. Phys. Chem. C* **115**, 18589 (2011)
- M. Inaba, in *Polymer electrolyte fuel cell durability*, ed. by F. N. Büchi, M. Inaba, T. J. Schmidt. (Springer, New York, 2009), p. 61
- S. Mukerjee, S. Srinivasan, in *Handbook of fuel cells fundamentals, fundamentals, technology, and applications*, ed. by W. Vielstich, A. Lamm, H. A. Gasteiger. (John Wiley & Sons, Chichester, 2003), p. 502
- L. Gan, P. Strasser, in *Electrocatalysis in fuel cells*, ed. by M. Shao. (Springer-Verlag, London, 2013), p. 541
- M. Mavrikakis, B. Hammer, J.K. Nørskov, *Phys. Rev. Lett.* **81**, 2819 (1998)
- J.R. Kitchin, J.K. Nørskov, M.A. Barteau, J.G. Chen, *J. Chem. Phys.* **120**, 10240 (2004)
- J.K. Nørskov, J. Rossmeisl, A. Logadottir, L. Lindqvist, J.R. Kitchin, T. Bligaard, H. Jónsson, *J. Phys. Chem. B* **108**, 17886 (2004)
- V. Čolic, A.S. Bandarenka, *ACS Catal.* **6**, 5378 (2016)
- V.R. Stamenkovic, B.S. Mun, K.J.J. Mayrhofer, P.N. Ross, N.M. Markovic, J. Rossmeisl, J. Greeley, J.K. Nørskov, *Angew. Chem. Int. Ed.* **45**, 2897 (2006)
- V.R. Stamenkovic, B.S. Mun, M. Arenz, K.J.J. Mayrhofer, C.A. Lucas, G. Wang, P.N. Ross, N.M. Markovic, *Nat. Mater.* **6**, 241 (2007)
- T. Yoshida, K. Kojima, *Electrochem. Soc. Interface* **24**(2), 45 (2015)
- K. Kojima, K. Fukazawa, *ECS Trans.* **69**(17), 213 (2015)
- L. Xiong, A. Manthiram, *J. Electrochem. Soc.* **152**, A697 (2005)
- D. Wang, H.L. Xin, R. Hovden, H. Wang, Y. Yu, D.A. Muller, F.J. DiSalvo, H.D. Abruña, *Nat. Mater.* **12**, 81 (2013)
- P.J. Ferreira, G.J. la O', Y. Shao-Horn, D. Morgan, R. Makharia, S. Kocha, H.A. Gasteiger, *J. Electrochem. Soc.* **152**, A2256 (2005)
- K. Yasuda, A. Taniguchi, T. Akita, T. Ioroi, Z. Shiroma, *Phys. Chem. Chem. Phys.* **8**, 746 (2006)
- S.S. Kocha, in *Polymer electrolyte fuel cell degradation*, ed. by M. M. Mench, E. C. Kumbur, T. N. Veziroglu. (Academic Press, Waltham, 2012), p. 174
- F. Hiraoka, K. Matsuzawa, S. Mitsushima, *Electrocatalysis* **4**, 10 (2013)
- A.C.C. Tseung, S.C. Dhara, *Electrochim. Acta* **20**, 681 (1975)
- Y. Shao-Horn, W.C. Sheng, S. Chen, P.J. Ferreira, E.F. Holby, D. Morgan, *Top. Catal.* **46**, 285 (2007)
- L. Gan, P. Strasser, in *Electrocatalysis in fuel cells*, ed. by M. Shao. (Springer-Verlag, London, 2013), p. 553
- P. Yu, M. Pemberton, P. Plasse, *J. Power Sources* **144**, 11 (2005)
- S. Chen, H.A. Gasteiger, K. Hayakawa, T. Tada, Y. Shao-Horn, *J. Electrochem. Soc.* **157**, A82 (2010)
- Y. Hoshi, E. Tada, A. Nishikata, T. Tsuru, *Electrochim. Acta* **85**, 268 (2012)
- A. Ooi, E. Tada, A. Nishikata, *J. Electrochem. Soc.* **163**, F1558 (2016)
- A. Ooi, E. Tada, A. Nishikata, *J. Electrochem. Soc.* **164**, C104 (2017)
- C.A. Reiser, L. Bregoli, T.W. Patterson, J.S. Yi, J.D. Yang, M.L. Perry, T.D. Jarvi, *Electrochem. Solid-State Lett.* **8**, A273 (2005)

42. Y. Sugawara, T. Okayasu, A.P. Yadav, A. Nishikata, T. Tsuru, J. Electrochem. Soc. **159**, F779 (2012)
43. A. Proctor, P.M.A. Sherwood, Anal. Chem. **54**, 13 (1982)
44. Powder Diffraction File (PDF) Card No. 00–029–0498 and 01–071–7407
45. M. Pourbaix, *Atlas of electrochemical equilibria in aqueous solutions*, 2nd edn. (NACE, Houston, 1974), p. 324 and 379
46. N. Todoroki, Y. Iijima, R. Takahashi, Y. Asakimori, T. Wadayama, J. Electrochem. Soc. **160**, F591 (2013)
47. P. Kiatkittikul, J. Yamaguchi, T. Nohara, R. Hagiwara, Electrochemistry **84**, 766 (2016)
48. M. Wakisaka, S. Mitsui, Y. Hirose, K. Kawashima, H. Uchida, M. Watanabe, J. Phys. Chem. B **110**, 23489 (2006)
49. D.F. van der Vliet, C. Wang, D. Li, A.P. Paulikas, J. Greeley, R.B. Rankin, D. Strmcnik, D. Tripkovic, N.M. Markovic, V.R. Stamenkovic, Angew. Chem. Int. Ed. **51**, 3139 (2012)
50. Y. Huang, F.T. Wagner, J. Zhang, J. Jorné, J. Electrochem. Soc. **161**, F653 (2014)
51. B.E. Conway, Prog. Surf. Sci. **49**, 331 (1995)
52. G. Jerkiewicz, G. Vatankhah, J. Lessard, M.P. Soriaga, Y.S. Park, Electrochim. Acta **49**, 1451 (2004)
53. A. Sun, J. Franc, D.D. Macdonald, J. Electrochem. Soc. **153**, B260 (2006)
54. H. Imai, K. Izumi, M. Matsumoto, Y. Kubo, K. Kato, Y. Imai, J. Am. Chem. Soc. **131**, 6293 (2009)
55. M. Tada, S. Murata, T. Asakoka, K. Hiroshima, K. Okumura, H. Tanida, T. Uruga, H. Nakanishi, S. Matsumoto, Y. Inada, M. Nomura, Y. Iwasawa, Angew. Chem. Int. Ed. **46**, 4310 (2007)
56. M.F. Mathias, R. Makharia, H.A. Gasteiger, J.J. Conley, T.J. Fuller, C.J. Gittleman, S.S. Kocha, D.P. Miller, C.K. Mittelsteadt, T. Xie, S.G. Yan, P.T. Yu, Electrochem. Soc. Interface **14**(3), 24 (2005)
57. K.C. Neyerlin, R. Srivastava, C. Yu, P. Strasser, J. Power Sources **186**, 261 (2009)
58. E. Antolini, J.R.C. Salgado, E.R. Gonzalez, J. Power Sources **160**, 957 (2006)
59. L. Dubau, F. Maillard, M. Chatenet, L. Guetaz, J. André, E. Rossinot, J. Electrochem. Soc. **157**, B1887 (2010)
60. S. Chen, P.J. Ferreira, W. Sheng, N. Yabuuchi, L.F. Allard, Y. Shao-horn, J. Am. Chem. Soc. **130**, 13818 (2008)
61. S. Chen, W. Sheng, N. Yabuuchi, P.J. Ferreira, L.F. Allard, Y. Shao-horn, J. Phys. Chem. C **113**, 1109 (2009)
62. C. Wang, M. Chi, D. Li, D. Strmcnik, D. van der Vliet, G. Wang, V. Komanicky, K.C. Chang, A.P. Paulikas, D. Tripkovic, J. Pearson, K.L. More, N.M. Markovic, V.R. Stamenkovic, J. Am. Chem. Soc. **133**, 14396 (2011)
63. X. Wang, R. Kumar, D.J. Myers, Electrochem. Solid-State Lett. **9**, A225 (2006)
64. V. Komanicky, K.C. Chang, A. Menzel, N.M. Markovic, H. You, X. Wang, D. Myers, J. Electrochem. Soc. **153**, B446 (2006)
65. R.K. Ahluwalia, S. Arisetty, X. Wang, X. Wang, R. Subbaraman, S.C. Ball, S. DeCrane, D.J. Myers, J. Electrochem. Soc. **160**, F447 (2013)
66. K. Kinoshita, J.T. Lundquist, P. Stonehart, J. Electroanal. Chem. **48**, 157 (1973)
67. A.A. Topalov, I. Katsounaros, M. Auinger, S. Cherevko, J.C. Meier, S.O. Klemm, K.J.J. Mayrhofer, Angew. Chem. Int. Ed. **51**, 12613 (2012)
68. A.A. Topalov, S. Cherevko, A.R. Zeradjanin, J.C. Meier, I. Katsounaros, K.J.J. Mayrhofer, Chem. Sci. **5**, 631 (2014)
69. S. Cherevko, N. Kulyk, K.J.J. Mayrhofer, Nano Energy **29**, 275 (2016)
70. L. Xing, G. Jerkiewicz, D. Beauchemin, Anal. Chim. Acta **785**, 16 (2013)
71. L. Xing, M.A. Hossain, M. Tian, D. Beauchemin, K.T. Adjemian, G. Jerkiewicz, Electrocatalysis **5**, 96 (2014)
72. S. Mitsushima, S. Kawahara, K. Ota, N. Kamiya, J. Electrochem. Soc. **154**, B153 (2007)
73. M. Umeda, T. Maruta, M. Inoue, A. Nakazawa, J. Phys. Chem. C **112**, 18098 (2008)
74. Y. Sugawara, A.P. Yadav, A. Nishikata, T. Tsuru, Electrochemistry **75**, 359 (2007)
75. Y. Sugawara, A.P. Yadav, A. Nishikata, T. Tsuru, J. Electroanal. Chem. **662**, 379 (2011)
76. Z. Wang, E. Tada, A. Nishikata, J. Electrochem. Soc. **161**, F380 (2014)
77. Z. Wang, E. Tada, A. Nishikata, Mater. Trans. **56**, 1214 (2015)
78. Y. Furuya, T. Mashio, A. Ohma, N. Dale, K. Oshihara, G. Jerkiewicz, J. Chem. Phys. **141**, 164705 (2014)
79. Z. Gu, P.B. Balbuena, J. Phys. Chem. C **111**, 9877 (2007)
80. Z. Gu, P.B. Balbuena, J. Phys. Chem. C **111**, 17388 (2007)
81. M. Wakisaka, S. Asizawa, H. Uchida, M. Watanabe, Phys. Chem. Chem. Phys. **12**, 4184 (2010)
82. D.C. Johnson, D.C. Napp, S. Bruckenstein, Electrochim. Acta **15**, 1493 (1970)
83. A.P. Yadav, A. Nishikata, T. Tsuru, J. Electrochem. Soc. **156**, C253 (2009)
84. Z. Wang, E. Tada, A. Nishikata, J. Electrochem. Soc. **163**, F421 (2016)
85. S. Siegel, H.R. Hoekstra, B.S. Tani, J. Inorg. Nucl. Chem. **31**, 3803 (1969)
86. T. Shimazaki, T. Suzuki, M. Kubo, Theor. Chem. Accounts **130**, 1031 (2011)
87. H. Imai, M. Matsumoto, T. Miyazaki, K. Kato, H. Tanida, T. Uruga, Chem. Commun. **47**, 3538 (2011)
88. Z. Gu, P.B. Balbuena, J. Phys. Chem. C **112**, 5057 (2008)
89. P. Mathew, J.P. Meyers, R. Srivastava, P. Strasser, J. Electrochem. Soc. **159**, B554 (2012)